Received: 11 August 2020 | Accepted: 8 October 2020

DOI: 10.1002/jemt.23625

RESEARCH ARTICLE

MICROSCOPY RESEARCH & TECHNIQUE WILEY

An experimental method to characterize the relationship between aperture image and ray directions in microscope optics

Mai Thi Tran[1,2] | Rudolf Oldenbourg[2]

[1]College of Engineering and Computer Science, VinUniversity, Hanoi, Vietnam

[2]Marine Biological Laboratory, Woods Hole, Massachusetts

Correspondence
Mai Thi Tran, College of Engineering and Computer Science, VinUniversity, Gia Lam District, Hanoi, Vietnam.
Email: mai.tt@vinuni.edu.vn

Funding information
The National Institute of General Medical Sciences, Grant/Award Numbers: R01GM114274, R35GM131843

Review Editor: Alberto Diaspro

Abstract

We propose a direct experimental method to calibrate the relationship between ray directions in object space and their positions in the aperture plane of a light field microscope. The calibration improves the interpretation of light field images, which contain information from both types of image planes, the field plane and the aperture plane of the ray path in the microscope. Our method is based on the diffraction of line gratings of known periodicities and provides accurate results with subpixel resolution. The method can be custom-tailored to most any optical configuration, including standard light microscopy setups, whenever correct mapping between ray parameters in the object/image plane and the aperture plane is needed.

KEYWORDS

aperture image, birefringence, light field microscope, line grating, microlens array, polarized light, polarized light field microscope

1 | INTRODUCTION

In this article, we present an experimental method for calibrating the relationship between the directions of rays in object space and their position in the aperture plane of microscope optics. By way of explanation, in the optical train of a microscope, one can identify two sets of planes that are called field planes and aperture planes (Oldenbourg & Shribak, 2010). Field planes include the object and image plane, while the back focal plane of the objective lens represents an aperture plane in the optical train. The two sets of planes are related to each other by a Fourier transform. When using geometric or ray optics to describe image formation in the microscope, a Fourier transform relates the position and angular direction of a ray in the object plane to an angular direction and position of the same ray in the aperture plane. Note the reciprocity here, all rays that originate in or pass through a point in the object plane have the same angular direction through the aperture plane, while all rays that have the same direction anywhere through the object plane are all focused into a point in the aperture plane. Hence, the light radiation through either plane can be described by a 4D light field represented by the 2D positional and 2D angular coordinates of the set of rays passing through both types of planes.

The light field microscope, first introduced by Mark Levoy and colleagues in 2006 (Levoy, Ng, Adams, Footer, & Horowitz, 2006), records the 4D light field in the image plane of a standard wide field microscope by placing a microlens array in the image plane, where usually the camera sensor is located. Instead, the camera is moved a short distance behind the array, into the back focal plane of the microlenses. Hence, the light field image recorded by this combination of microlens array and camera represents the distribution of image rays in their positions and angles in the image plane. While the position of a ray that passes through a microlens is encoded by the position of the microlens in the array, the directional angles of the ray are encoded in its position in the aperture image behind the microlens. Since its inception in 2006, light field microscopy has attracted much attention because it enables the reconstruction of 3D spatial object parameters such as fluorescence density and local absorption coefficients in a single snapshot (Cong et al., 2017; Huang et al., 2018; Li et al., 2019; Prevedel et al., 2014; Wagner et al., 2019). As outlined in Levoy's original publication, the positional and angular information retained in a light field image can in fact be

converted into 3D image data in several ways, such as a conventional focus stack through object space, or pans of extended focus projections of the object scene along a multitude of viewing directions. In more general terms, a light field image can be processed like a limited angle tomographic data set (Tian & Waller, 2015). It needs to be said, however, while recording the light field in this way retains the option of reconstructing a 3D object scene, it does so by reducing the resolution that is usually available in the native image plane of a given objective lens when the camera is placed in its image plane directly. In other words, light field imaging trades some of the 2D spatial resolution in the native image plane for the ability to reconstruct 3D object parameters using a single snapshot. And yet, there are several groups who are addressing this trade-off and uneven resolution that hold back light field microscopy, and are developing new processing algorithms that minimize artifacts and speed up reconstruction (Guo, Liu, Hua, Li, & Jia, 2019; Stefanoiu, Page, Symvoulidis, Westmeyer, & Lasser, 2019).

In polarized light microscopy, the trade-off has been accepted for a long time if the ultimate goal is to measure the birefringence or three-dimensional anisotropy indicatrix of crystals, for example. In the conventional polarized light microscope, one can measure the azimuth angle of a birefringent structure whose optic axis is oriented in the image plane of the microscope. However, the inclination angle of the optic axis remains hidden in the regular, so-called orthoscopic image. To reveal the inclination angle, which is the angle by which the optic axis is rotated out of the image plane, one needs to add the so-called Bertrand lens to the optical train to project the image of the back focal plane of the objective lens onto the eye or camera. This so-called conoscopic image is known to reveal the type of indicatrix, such as uniaxial or biaxial, and the inclination angle of the optic axis for a single crystal under observation (Hartshorne & Stuart, 1960). Hence, a polarized light field image merges the conoscopic and orthoscopic views of traditional polarized light microscopy and can be analyzed for the three-dimensional anisotropy indicatrix of many small crystals or ordered structures, all at once (Oldenbourg, 2008).

We are now proposing an experimental method to calibrate the relationship between ray angles in the object plane and ray positions in the aperture plane of a light field microscope. This calibration is important when analyzing light field images for all 3D object parameters, but especially so when measuring anisotropic objects, whose parameters like the refractive index depend on the direction and polarization of light rays transmitted through object space (Tran & Oldenbourg, 2018). As we are developing algorithms for reconstructing object parameters based on polarized light field images, we are relying on the correct mapping between ray parameters in the object/image plane and the aperture plane. Because this mapping does depend on the exact placement of the microlens and camera sensors with respect to each other and the rest of the imaging components, it is best to measure this calibration directly instead of relying on calculations based on indirect measurements and manufacturers' specifications.

The article is organized as follows: We first describe the test sample and the optical setup. Then we give a detailed description of the calibration method based on light field images of line gratings. We demonstrate the utility of the approach to calibrate the aperture image of a light field microscope. Notably, the relationship between the ray's tilt

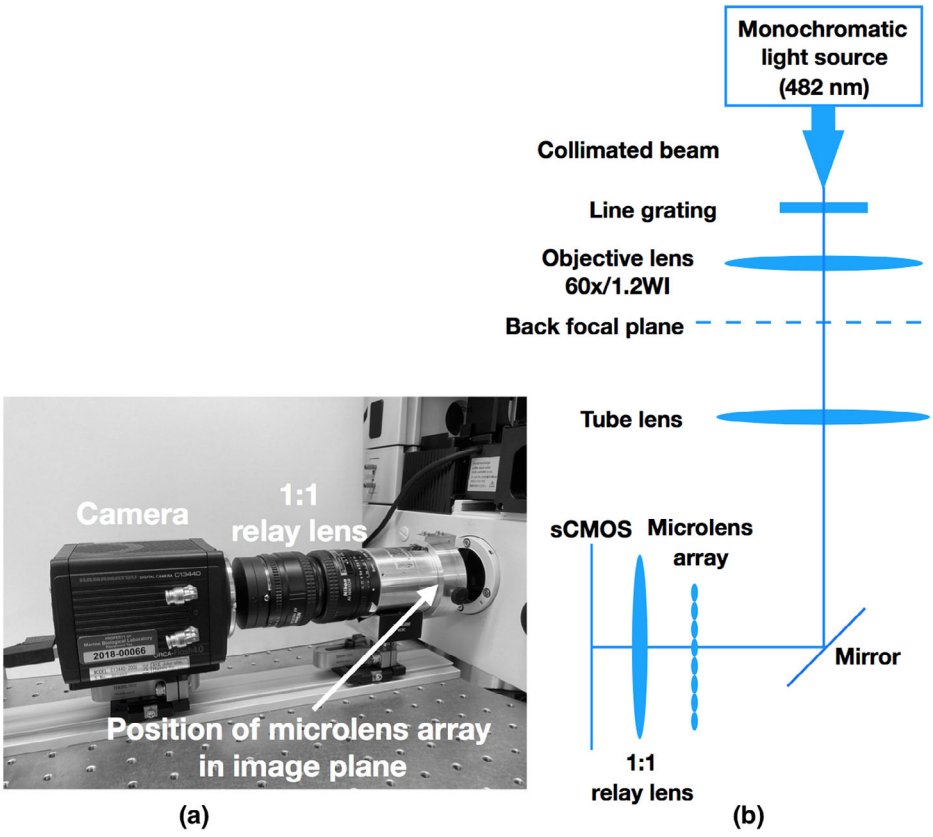

FIGURE 1 (a) Light field camera at the left side port of the inverted Nikon Ti microscope stand used in this study. (b) Schematic of the optical setup, including the combination of microlens array—1:1 relay lens—camera. The relay lens projects a 1:1 image of the microlens back focal plane onto the camera sensor [Color figure can be viewed at wileyonlinelibrary.com]

angle and the ray's position in the aperture image is carefully described. This article also characterizes three aperture images corresponding to the different objective lenses, microlens arrays, and the CCDs. In the last section, the applications of our method will be discussed.

2 | MATERIALS AND METHODS

2.1 | Optical setup

The light field microscope we use in our experiments consists of a traditional wide field setup in which the regular camera is replaced by a light field camera. A schematic of the optical setup is shown in Figure 1, which includes a photo of the light field camera (Figure 1a). For convenience, the assembly includes a 1:1 relay lens (two AF Nikkor 50mm f/1.4D mounted nose to nose; Nikon, Melville, NY) that projects the back focal plane of the microlens array onto the sensor of a commercial camera. We employed either one of two microlens arrays, depending on the microscope objective lens used for imaging. For the current project we used a 60x/1.4NA oil immersion and a 60x/1.2NA water immersion Plan Apo objective lens. The 60x/1.4NA oil objective is typically paired with a microlens array of 125 μm pitch and 2.5 mm focal length, in which the f-Number of each microlens nearly matches the imaging side NA = 1.4/60 = 0.023 of the oil immersion objective. For the water immersion objective with a slightly lower NA, we use a microlens array with 100 μm pitch and 2.5 mm focal length. The arrays of square microlenses have a 100% fill factor and were fabricated by RPC Photonics (Rochester, NY) to our custom specifications. The microlens holder was fabricated in-house and mounted on an optical rail together with the relay lens and camera (Figure 1a). Images were recorded on one of two monochrome camera sensors, a CCD camera with 7.4 μm square pixels (Retiga, 4000R;

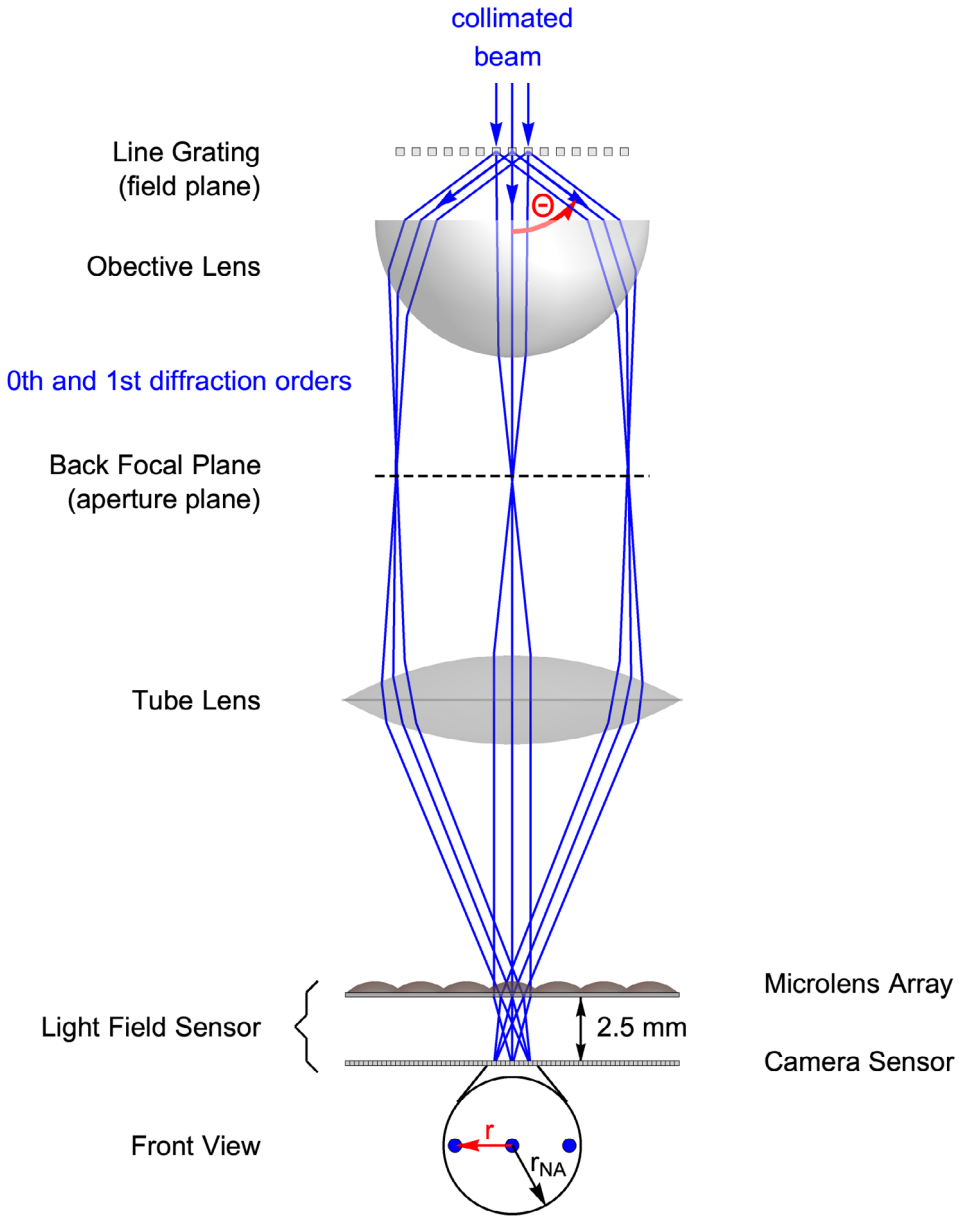

FIGURE 2 The schematic illustrates the light path of diffraction orders created by a line grating in the object/field plane and propagating through the microscope optics to the light field sensor. After passing through the grating, the straight zeroth-order beam travels parallel to the optical axis of the microscope, while the two first-order beams travel under a tilt angle Θ and are focused into points that are a distance r from the zeroth-order point in the aperture image behind a microlens. r_{NA} is the radius of the edge of the aperture of the objective lens with the numerical aperture NA [Color figure can be viewed at wileyonlinelibrary.com]

QImaging, Surrey BC, Canada) and a sCMOS camera with 6.5 μm square pixels (ORCA-Flash4.0; Hamamatsu Photonics, Bridgewater, NJ).

As wide field microscope we used an inverted stand (Ti-E) with optics from Nikon, including a halogen light source, interference filter (482/18nm, BrightLine; Semrock/IDEX Corp., Lake Forest, Illinois) and condenser optics with nearly closed aperture diaphragm to achieve a monochromatic, collimated beam that trans-illuminated the line gratings (Figure 1b).

After the collimated beam passed through the line gratings, the diffracted light is collected by the objective lens, which projects an image of the gratings into the image plane at the left side port of the inverted stand. The aforementioned light field camera was positioned in such a way that the microlens array was placed in the image plane of the microscope's optical train.

In addition to the light field configuration, the assembly can be reconfigured to record standard, high-resolution microscope images by simply moving the microlens array axially in the following way. As shown in the photo of Figure 1a, the microlens array is mounted in a holder that is attached to the relay lens, which in turn is attached to the camera body. The microlens holder is made of two concentric aluminum tubes, with the inner tube holding the microlens array. The inner tube can be moved along the optical axis of the microscope to precisely place the array into the image plane. In addition, the distance between the microlens array and the relay lens can be independently adjusted so as to image the back focal plane of the microlenses onto the camera sensor. These positions are marked and identified as the light field configuration. For recording standard, high-resolution microscope images, the microlens array is moved closer to the relay lens into the plane that is projected onto the camera sensor. In that second position, the microlenses themselves are imaged onto the camera and their overall effect almost disappears on the image of the object under observation (compare images in Figure 3a,b; see also Oldenbourg, 2008). Hence, with the same optical setup, the gratings can be imaged either in the standard imaging mode of the microscope optics or in the light field imaging mode, simply by moving the microlens array by a distance equal to the focal length of the microlenses (2.5 mm).

2.2 | Test sample

As test sample, we used line gratings with well-defined periodicities that are part of the MBL/NNF test target. This test/calibration target consists of a glass coverslip with a thin aluminum layer, into which several test patterns, including fine line gratings were etched using electron lithography. Individual line gratings with periodicities of 0.10,

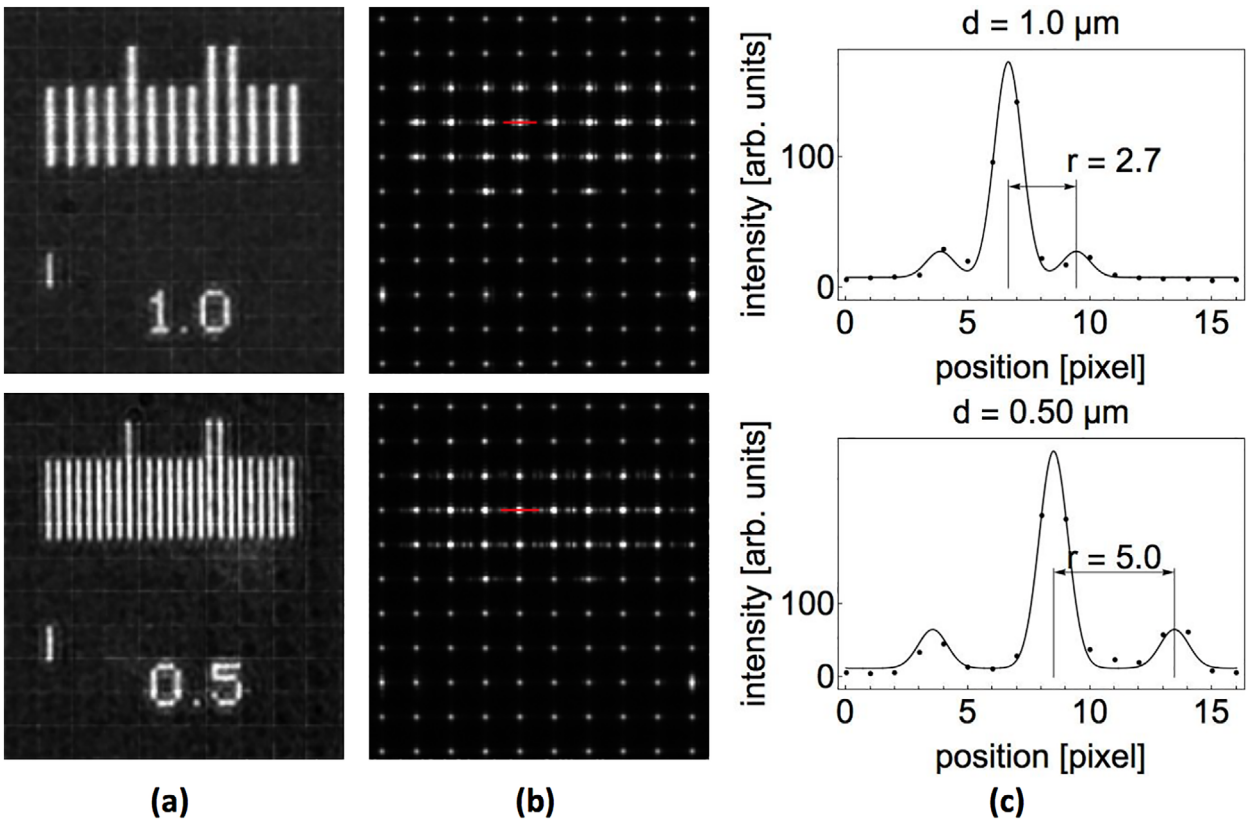

FIGURE 3 Line gratings of the MBL/NNF test target, imaged with (a) standard and (b) light field microscope. In (b), the collimated illumination beam, that is, condenser aperture nearly closed, is imaged into the center of the aperture image behind each microlens, while the first-order diffraction is visible as two subsidiary maxima. The horizontal red lines identify the pixels whose recorded intensities are shown as data points in the profiles of (c). The continuous lines in the graphs represent the best fit applied to the data to determine the distance *r* between the central and subsidiary maxima. The contrast was enhanced [Color figure can be viewed at wileyonlinelibrary.com]

0.15, 0.17, 0.2, 0.25, 0.29, 0.33, 0.4, 0.5, 1.0, and 2.0 μm are available (Oldenbourg et al., 1996).

2.3 | Calibration of aperture images

Our aim is to find the relationship between the direction of rays in object space and their position in the aperture plane in recorded light field images. The direction of a ray in object space can be defined by an azimuth angle in the field plane and a tilt angle with respect to the normal of the field plane. To find the azimuth angle, the vector representing the ray direction is first projected into the field plane and then the angle between the projection and a reference axis, for example the *x*-axis of a Cartesian coordinate system, is taken to be the azimuth angle. The same azimuth angle can also be found in the aperture plane as the angle between the direction defined by the point where the ray passes through the aperture plane, the center of the aperture plane, and the direction in the aperture plane that corresponds to the *x*-direction in the field plane. Hence, the azimuth angle appears in both, the field and aperture planes, as the same angle in each plane. However, the tilt angle Θ in object space is related to the distance *r* between the point where the ray passes through the aperture plane and the center of the aperture plane (see Figure 2). Hence, the cone shaped distribution of rays in object space that enter the objective lens is transformed into a disk with radius r_{NA} in the aperture plane, with r_{NA} corresponding to the maximum tilt angle Θ_{max} of rays that are still accepted by the objective lens. In the remainder of this section, our aim will be to establish the relationship between Θ and *r*, and express it in known or measurable quantities.

To find the relationship between Θ and *r*, we use the fact that microscope objectives are designed to fulfill Abbe's sine condition, an important requirement for imaging optics to minimize off-axis spherical aberration and coma (Oldenbourg & Shribak, 2010). This design feature leads to the expression,

$$r = \text{const} \cdot \sin\Theta, \quad (1)$$

where const has the dimension of a distance and our task is to find the value of const for a given imaging system and aperture plane. From Figure 2, it is apparent that the value of const is much bigger when considering the back focal plane of the objective lens as the aperture plane, compared to the back focal plane of a microlens, which images the objective back focal plane, but at a much smaller scale.

A similar relationship exists between the maximum tilt angle that is still accepted by the objective's front lens, and the numerical aperture or NA of the objective lens: $NA = n \cdot \sin\Theta_{NA}$. *n* is the refractive index of the immersion medium and Θ_{NA} is the maximum tilt angle in the medium. Next, we write r_{NA} for the radius that corresponds to the maximum tilt angle and use expression (1) to write $r_{NA} = \text{const} \cdot \sin\Theta_{NA}$. Then, we replace $\sin\Theta_{NA}$ with NA/*n* and solve for const,

$$\text{const} = r_{NA} \cdot n / \text{NA}. \quad (2)$$

Now we have an expression for const with the known parameters *n* and NA, and the radius r_{NA} that can be measured for a given optical system and aperture plane.

Behind each microlens in our light field sensor, there is a square array of approximately 17 by 17 pixels. Hence, the spatial resolution of the disk-shaped aperture image behind a microlens is not enough to clearly discern the edge of the disk or its radius r_{NA}. Furthermore, in transmitted light microscopy, the aperture of the objective is not necessarily fully illuminated because of partial vignetting or stops in the illuminating beam. Therefore, we are employing line gratings of known periodicity to establish more precisely the relationship between the tilt angle in object space and its radius position in the aperture plane. With expressions (1) and (2) in mind, this is equivalent to more precisely determining r_{NA} for a given optical setup.

3 | RESULTS AND DISCUSSIONS

To create rays of known tilt angles in object space, we used line gratings of known periodicities. Rays that generate the zeroth and first diffraction orders travel in well-defined directions with the respect to the incoming collimated beam of light. Rays of the zeroth order travel in the same direction as the incoming beam, while rays of the first

TABLE 1 The measured distance r between zero and first diffraction maxima depends on the periodicity d of the grating and the corresponding diffraction angle

d (μm)	sinΘ	*r* (pixel)	SD
0.5	0.725	4.98	0.14
1	0.362	2.74	0.12
∝	0	0	0

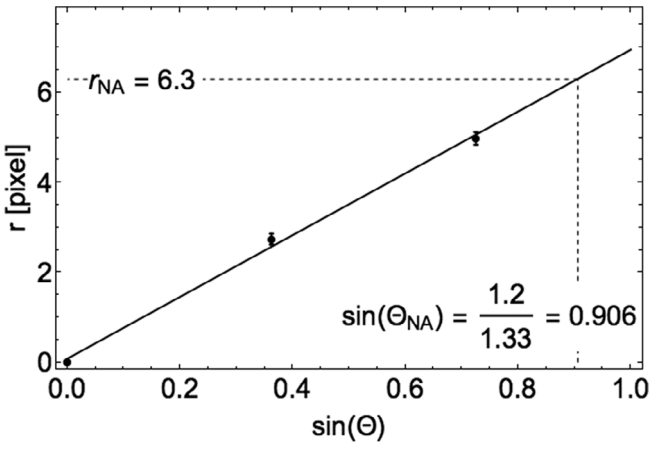

FIGURE 4 Graph representing the measured distance *r* between zero and first diffraction maxima (see Figure 3c) and the diffraction angle Θ derived with expression (2). Data points and error bars represent means and standard deviations of five measurements each

Objective lens	Microlens array	Camera	r_{NA} (pixel)
60x/1.4 NA oil	125 μm pitch/2,500 μm focal length	QCam: 7.4 μm/pixel	7.25
60x/1.2 water	125 μm pitch/2,500 μm focal length	QCam: 7.4 μm/pixel	6.3
60x/1.2 water	100 μm pitch/2,500 μm focal length	Orca Flash4: 6.5 μm/pixel	7.7

TABLE 2 The value of r_{NA} for three different setups

diffraction order are tilted with respect to that direction by an angle Θ defined by the wavelength λ of the light and the periodicity d of the grating: $\sin\Theta = \lambda_{medium}/d$. The wavelength λ_{medium} is that of the light in the medium in which the grating is embedded. In a medium with refractive index n, the wavelength is reduced by a factor $1/n$ compared to the wavelength λ in vacuum; hence, when using λ in vacuum, the relationship becomes,

$$\sin\Theta = \lambda/(n \cdot d). \quad (3)$$

Figure 3 shows results for line gratings with periodicities of 1.0 and 0.5 μm, which were imaged with the optical setup in Figure 1, using light of wavelength 482 nm, the 60x/1.2NA objective lens, and Retiga 4000R CCD camera from QImaging. For recording the images in (a), the microlens array was moved to the position for standard, high-resolution imaging (see section 2.1). The images in (b) show light field images of the same gratings, now with the microlens array in the position that projects the aperture images onto the camera sensor. In (b), behind each microlens, the collimated illumination beam is focused into the center of the aperture images, with the top two rows of aperture images also featuring the subsidiary diffraction maxima of the gratings whose images fall on the respective microlenses. Figure 3c shows horizontal intensity profiles along lines that are indicated in red in (b). The intensity profiles clearly show the central maximum and two subsidiary maxima symmetric in position to the central one and increasing in distance with decreasing grating pitch.

The continuous lines in the graphs of Figure 3c represent the best fit using least square regression of the data points to a sum of three Gaussian curves, one representing the central line and two, spaced symmetrically to the central line, representing the first-order diffraction maxima. For each line grating there were five aperture images, that is, five microlenses that covered the grating. This allowed us to determine the mean and standard deviation of the measured distance r. Table 1 shows the corresponding values in Figure 3c. In Figure 4, the data pairs ($\sin\Theta$, r) are plotted in a graph that is extended by a linear fit to the value of $\sin\Theta_{NA}$ that corresponds to the NA of the objective lens used. This approach gives r_{NA} = 6.3 for the water immersion lens with NA = 1.2. Hence, the linear fit through the data points in Figure 4 is a graphical representation of expression (1) with const = $r_{NA} \cdot NA/n$ = 5.68 for the optical setup using the given objective lens, microlens array and camera sensor. Based on this method, we measured the value of r_{NA} for three different setups whose specifications and measured r_{NA} values are summarized in Table 2.

4 | CONCLUSIONS

We have described a method to calibrate the back focal plane of the objective lens of an imaging system in terms of the direction of rays and their positions in object space. This relationship between points in the field and aperture plane is especially important in light field imaging, where information from both planes are culled to reconstruct object parameters over a considerable depth of field, including their orientation based on their anisotropic response. As a multiview imaging modality, polarized light field microscopy has the potential to recover the 3D anisotropy such as the birefringence and optic axis orientation of anisotropic materials, tissues, and cell structures, at high spatial and orientational resolution (Tran & Oldenbourg, 2018). With light field microscopy making inroads into many application areas, we believe that providing a consistent metric between all measured quantities of a light field is important to improve the accuracy and consistency of measured object features.

ACKNOWLEDGMENTS

This work was supported by the National Institute of General Medical Sciences through grant numbers: R01GM114274 and R35GM131843.

ORCID

Mai Thi Tran https://orcid.org/0000-0002-7993-5735

REFERENCES

Cong, L., Wang, Z., Chai, Y., Hang, W., Shang, C., Yang, W., … Wen, Q. (2017). Rapid whole brain imaging of neural activity in freely behaving larval zebrafish (*Danio rerio*). *eLife*, *6*, e28158.

Guo, C., Liu, W., Hua, X., Li, H., & Jia, S. (2019). Fourier light-field microscopy. *Optics Express*, *27*(18), 25573–25594.

Hartshorne, N. H., & Stuart, A. (1960). *Crystals and the polarising microscope: A handbook for chemists and others*. London, United Kingdom: Arnold.

Huang, X., Qi, H., Zhang, X.-L., Ren, Y.-T., Ruan, L.-M., & Tan, H.-P. (2018). Application of Landweber Method for 3D Temperature Field Reconstruction Based on the Light-Field Imaging Technique. *Journal of Heat Transfer*, *140*, 082701.

Levoy, M., Ng, R., Adams, A., Footer, M., & Horowitz, M. New York, USA: The Association for Computing Machinery; (2006). Light field microscopy. In *ACM SIGGRAPH 2006 papers* (pp. 924–934).

Li, H., Guo, C., Kim-Holzapfel, D., Li, W., Altshuller, Y., Schroeder, B., … Takamaru, K.-I. (2019). Fast, volumetric live-cell imaging using high-resolution light-field microscopy. *Biomedical Optics Express*, *10*(1), 29–49.

Oldenbourg, R. (2008). Polarized light field microscopy: An analytical method using a microlens array to simultaneously capture both conoscopic and orthoscopic views of birefringent objects. *Journal of Microscopy*, *231*(3), 419–432.

Oldenbourg, R., Inoué, S., Tiberio, R., Stemmer, A., Mei, G., & Skvarla, M. (1996). *Standard test targets for high resolution light microscopy*. Cambridge, United Kingdom: Cambridge University Press.

Oldenbourg, R., & Shribak, M. New York, USA: McGRAW-HILL, INC; (2010). Microscopes. In *Handbook of optics* (Vol. 1, pp. 21–28).

Prevedel, R., Yoon, Y.-G., Hoffmann, M., Pak, N., Wetzstein, G., Kato, S., … Boyden, E. S. (2014). Simultaneous whole-animal 3D imaging of neuronal activity using light-field microscopy. *Nature Methods*, *11*(7), 727–730.

Stefanoiu, A., Page, J., Symvoulidis, P., Westmeyer, G. G., & Lasser, T. (2019). Artifact-free deconvolution in light field microscopy. *Optics Express*, *27*(22), 31644–31666.

Tian, L., & Waller, L. (2015). 3D intensity and phase imaging from light field measurements in an LED array microscope. *Optica*, *2*(2), 104–111.

Tran, M. T., & Oldenbourg, R. (2018). Mapping birefringence in three dimensions using polarized light field microscopy: The case of the juvenile clamshell. *Journal of Microscopy*, *271*(3), 315–324.

Wagner, N., Norlin, N., Gierten, J., de Medeiros, G., Balázs, B., Wittbrodt, J., … Prevedel, R. (2019). Instantaneous isotropic volumetric imaging of fast biological processes. *Nature Methods*, *16*(6), 497–500.

How to cite this article: Tran MT, Oldenbourg R. An experimental method to characterize the relationship between aperture image and ray directions in microscope optics. *Microsc Res Tech*. 2020;1–7. https://doi.org/10.1002/jemt.23625